Heterogeneous local straining behavior under monotonic and cyclic loadings in a friction stir welded aluminum alloy

Keywords

Friction stir welding, Digital image correlation (DIC), Fatigue, Local strain, Crack initiation

Yasuko Besel[a)*], Michael Besel[a), 1)], Eric Dietrich[a)], Janine Wischek[a)], Ulises Alfaro Mercado[a)], Toshifumi Kakiuchi[b)], Yoshihiko Uematsu[b)]

a) German Aerospace Center (DLR), Institute of Materials Research, Linder Hoehe, 51147 Cologne, Germany

*yasuko.besel@dlr.de, +49-(0)2203-601-4078

b) Gifu University, Faculty of Engineering, Department of Mechanical Engineering, 1-1 Yanagido, Gifu 501-1193, Japan

1) present, Otto Fuchs KG

Abstract

Local strain evolution under monotonic and fatigue loadings was investigated in a friction stir welded (FSWed) Al-Mg-Sc alloy. The microstructure of the weld exhibited strong heterogeneity. Digital image correlation (DIC) technique was employed to evaluate local straining behavior in the weld seam in tensile testing. Onset of initial yielding was found locally near regions of lowest hardness. However, the local straining development didn't take place homogeneously in the stir zone (SZ) of the weld and constraints by surrounding microstructure affected further straining behavior in the weld. Local cyclic straining

behavior during fatigue loading was monitored in the same material using small strain gages. Fully reversed (R = -1) fatigue tests were conducted at a constant stress amplitude of σ_a = 220 MPa. Cyclic plastic strain found mainly on the advancing side of SZ in early fatigue phase contributed to initiation of fatigue cracks. Since fatigue crack initiation and the following propagation were also influenced by microstructure, hardness distribution or local straining evolution in tensile testing alone could not provide accurate prediction of fatigue fracture behavior of the weld.

Nomenclature

$\Delta\varepsilon_p$	plastic strain range
$\Delta\varepsilon_{pmax}$	maximum plastic strain range
$\Delta\sigma$	stress range
N	number of cycles
N_f	number of cycles to failure
R	stress ratio
σ_a	stress amplitude
$\sigma_{n,a}$	nominal stress amplitude
DIC	digital image correlation
FSW	friction stir weld
HAZ	heat affected zone
HCF	high cycle fatigue
SEM	scanning electron microscope
SZ	stir zone
TMAZ	thermo-mechanically affected zone
VHCF	very high cycle fatigue

1. Introduction

Friction stir welding (FSW) is a unique joining technique, which was invented and patented by TWI in 1991 [1]. FSW achieves solid-state joining and is applicable to metallic materials which show poor weldability by conventional welding methods like fusion welding. Precipitation hardening aluminum alloys of 2xxx and 7xxx series are well-known as non-fusion-weldable materials but can be welded by the FSW technique [2]. The FSW technique has been already widely implemented in various industrial fields, such as train, ship and aerospace manufacturing industries [1][3][4][5][6][7].

Through friction stir welding, two components are joined by stirring the workpiece materials with a rotating tool. The joining process is generally achieved below melting point of the material. The FSW technique requires no filler material, but strong plastic flow and heat during the process alter microstructure of the joint part from that of the base material. Spatial arrangements of the microstructure become complex and inhomogeneous near and in the FSWed joint. Typical FSWed joints of aluminum alloys consists of stir zone (SZ) in the center, thermo-mechanically affected zone (TMAZ) in the adjacent region and heat affected zone (HAZ) in the outer part [8]. Hardness, which is commonly evaluated as one of the mechanical properties of materials, generally differs in the weld area compared to the base material. The spatial distribution of the weld zones and hardness is not axisymmetric around the weld center line due to the asymmetric welding conditions on the advancing and retreating side. Such heterogeneity in microstructure and mechanical response of the friction stir welds depends on welding parameters and materials to be welded [2][9]. Some researchers have systematically investigated the effect of welding parameters in aluminum alloys [10][11][12][13]. Tool rotation speed as well as welding speed change shape of weld nuggets, affected grain sizes and hardness in the nuggets. Z-axis force of the welding tool is also an influencing factor for the quality of welds.

Such variety in characteristic features and strong inhomogeneity in the FS welds make it complicated to understand fracture behaviors of the weld joints under both monotonic and cyclic loadings. In order to analyze the local fracture behaviors, a digital image correlation (DIC) technique has recently been applied to some FSWed aluminum alloys [14][15][16][17][18][19]. The DIC technique enables quantitative evaluation of local straining behavior of a material under loading. Those studies showed development of inhomogeneous straining behavior causing fracture in the friction stir welds under monotonic loading.

Similar to the fracture behavior under monotonic loading, fatigue behavior can be influenced by the heterogeneity of the weld joints. In our past work [20], fatigue behavior of a friction stir welded Al-Mg-Sc alloy with three different welding speeds was investigated. The surface asperities produced during the FSW process such as flashes and tool marks were removed before the fatigue tests in that work since they

influence the fatigue crack initiation behavior. It was observed that fatigue cracks initiated mostly in the FSW stir zone but initiation sites were not limited to the lowest hardness region. Welding parameters influenced the microstructures of the welds which significantly affected the observed fatigue crack initiation behavior. Tortuous crack paths were formed due to the complex microstructures, and the applied stress levels influenced the crack initiation sites as well: at low stress levels, fatigue cracks are likely to initiate in the area with comparably complex microstructure on the retreating side. At high or medium stress levels, the fatigue cracks initiated extensively on the advancing side in the stir zone by locally concentrated yielding. However, the initiation sites at those stress levels were not located at the globally lowest hardness points of each specimen. That is, the local cyclic straining response, which plays an important role in fatigue crack initiation at high or medium stress levels, is not exclusively correlated to the local hardness but can also be influenced by other heterogeneities in the welds. Local cyclic straining evolution in a friction stir welded Al-Mg-Sc alloy with constant welding conditions was investigated in our previous work [21]. In that research, cyclic response of local straining behavior was directly monitored by taking an advantage of the strain gage technique. Although the applied nominal stress level was below the macroscopic yield point, local plastic straining was observed at several locations on the advancing side of the welds. The results implied that local cyclic plastic straining contributes to fatigue crack initiation in the welds. However, the influence of local straining behavior on fatigue behavior in the friction stir welded aluminum alloys have not been researched much as only a few publications can be found in literature, e.g. our previous work [21] and the attempt by Deng et al. [19]. Deng et al. have tried to investigate the correlation between micro mechanical property and fatigue crack initiation in the very high cycle fatigue (VHCF) regime in friction stir welded 7050 aluminum alloy. They conducted fatigue tests at the stress ratio R = -1 and observed an inflection point of the S-N curves of the FSW joints at around $\Delta\sigma$ = 180MPa in the VHCF regime. Micro mechanical property was analyzed under quasi static tensile loading by means of DIC technique. They suggested that the stress level of 180 MPa at which noticeable strain localization started to be observed during tensile testing coincided with the cyclic loading at the knee point of S-N curves. But the cyclic loading which they meant was the stress range of $\Delta\sigma$ =

180MPa where the maximum stress level becomes $\sigma_{max} = 90$MPa for $R = -1$. No further discussion of the difference between the (quasi-)static loading of 180 MPa and the cyclic loading with a stress range of $\Delta\sigma = 180$MPa was provided in [19]. Generally in conventional metallic materials, fatigue crack initiation is brought about by local irreversible cyclic slip deformation. Moreover, fatigue loading yields different straining situations in the material if compared to quasi static tensile loading. Thus, it is necessary to consider local straining behavior under cyclic loading as well as under tensile loading for detailed understanding of the fatigue crack initiation behavior in a heterogeneous material such as friction stir welds.

In this study, local straining behavior under monotonic loading in a friction stir welded Al-Mg-Sc alloy was investigated by DIC technique, while conventional strain gages were used to capture local straining under fatigue loading analogue our approach used in [21]. An Al-Mg-Sc alloy has been chosen because these alloys are promising candidates as next baseline material for metallic fuselage structures due to their slightly reduced density and corrosion resistance compared to the conventional fuselage materials like AA2024 [22]. Characteristic Al_3Sc precipitations in the Al-Mg-Sc alloys have high thermal stability and work as recrystallization inhibitor [23]. During friction stir welding of conventional aluminum alloys, dynamic recrystallization occurs in the majority of cases due to heat input and plastic flow [24][25][26]. It is expected in the FSWed Al-Mg-Sc alloys that the thermally stable Al_3Sc precipitations reduce degradation in mechanical properties, as already observed in some friction stir welded 2xxx alloys [27][28]. As mentioned above, in our current work fatigue tests were carried out and cyclic straining was measured at several locations in the weld region by means of strain gage technique. Then the correlation of heterogeneity of straining under monotonic loading and the local cyclic straining behavior under fatigue loading, which clearly attributed to fatigue crack initiation, is discussed.

2. Material and Experimental procedures

The material used in this study is 5024 Al-Mg-Sc alloy rolled plate with a thickness of 3.3 mm in H116 condition. The nominal chemical composition is listed in Table 1. Two plates were butted and friction stir welded. Before the FSW process the abutted surfaces of the plates were ground in order to minimize the effect of the native oxide layer on the weld joint quality. The friction stir tool had a conically threaded probe with a diameter of 4.5 mm and the shoulder with a diameter of 12.5 mm. The pin and the shoulder rotate together with the same rotational speed. The welding direction was parallel to the rolling direction of the plates. The welding parameters were chosen as tool rotation speed of 1200 rpm and travel speed of 720 mm/min, which were different from those in our previous work [21]. Before the tensile and fatigue tests, the basic quality of the weld joints was investigated by conducting root-bend tests in a three-point bend testing apparatus [29] and no root flaws were found. All tensile and fatigue tests described in the following section were conducted several months after the welding process, i.e. the microstructure is assumed to represent a (at least meta-) stable condition at ambient temperature. The specimens for the tensile and fatigue tests in the present work were prepared from the same batch of the FSWed plates as in our past work [20].

Tensile tests were performed with two types of strain measurements: a laser extensometer is used to obtain macroscopic tensile properties while DIC technique allows for local straining observation. Tensile test specimens were machined transverse to the welding direction with a parallel section length of 70 mm for both types of strain measurements. Any surface features of the weld such as weld flashes were not removed before tensile testing. For the laser extensometer measurement, the gage length was 30 mm and the crosshead speed was 1 mm/min. Fig. 1 shows the stress-strain curve obtained in the laser extensometer test and the evaluated tensile properties of this material are listed together with those of base material in Table 2. As seen in Fig. 1, this material exhibits serrations in the stress-strain curve after the yield point which is known as Portevin-Le Chatelier effect [30]. For the DIC observation, the through-thickness side surface of the weld was painted with a very fine stochastic black and white pattern. This enables local strain measurement with adequate resolution using an established commercial DIC program (GOM Correlate, see [31] for details). Local two-dimensional in-plane surface strains were evaluated with a

digital camera attached to an optical microscope. The camera used here was a digital single-lens reflex camera Canon EOS 70D with 20.2 million pixels (5472 × 3648 pixel^2) resolution. The observation area was about 17.1 × 11.4 mm^2. The crosshead speed was 0.5 mm/min and during testing 1 image was taken every 6 seconds. The facet size and the facet distance for the DIC analyses were set to 60 × 60 pixel^2 (ca. 188 × 188 μm^2) and 30 × 30 pixel^2 (ca. 94 × 94 μm^2) to allow local displacement and strain evaluation, respectively.

Fatigue tests were carried out under fully cyclic loading (R = -1) with the specimens as drawn in Fig. 2. Fatigue specimens are machined to have the FS-weld seam in the midst of the specimen. The loading axis is perpendicular to the weld line. Since the surface asperities produced during the FSW process such as flashes and tool marks could influence the fatigue crack initiation behavior (due to their notch-like effects), the surface layer was ground by emery papers followed by buff polishing with 1 μm-diamond suspension. The final thicknesses of the fatigue specimens were measured and, as a result, scattered in the range between 2.8 mm and 3.1 mm. In the current study, local strain during cyclic loading was monitored by attaching small foil strain gages (gage length of 1 mm and width of 1.1 mm) to the specimen surface. To ensure good adhesion of the strain gages, the specimen surface was slightly "scratched" with emery paper of grid #2000 after buff polishing applying only very low pressure to minimize magnitude and spatial extension of the unavoidably introduced residual stresses in the surface layer. The local cyclic strain was measured at 7 different locations around the weld seam as listed in Table 3 and schematically illustrated in Fig. 3 using 5 different specimens. Each strain gage was attached along the longitudinal centerline of the specimen. For practical reasons it was necessary to use different specimens as applying all strain gages to a single specimen would clearly have complicated its handling and fatigue testing beyond our tolerable degree. The strain in the direction parallel to the loading axis was monitored from the first loading cycle and up to 5,000 cycles. During the local strain measurements, the fatigue tests were conducted at 1 Hz and otherwise at 20 Hz. Load signal was recorded together with the strain signal using a data acquisition frequency of 100 Hz, i.e. 100 data points per cycle were obtained. These fatigue tests with local strain

measurements were performed at a constant stress amplitude of 220 MPa, which was slightly lower than the macroscopic 0.2 % yield stress of the FS weld seam, see Table 2.

Table 1 Chemical composition of Al-Mg-Sc alloy.

Chemical composition (wt.%)								
Si	**Fe**	**Cu**	**Zn**	**Mg**	**Mn**	**Ti**	**Sc**	**Al**
0.25	0.4	0.2	0.2	3.9	0.25	0.2	0.4	Bal.

Table 2 Tensile properties.

	0.2% yield stress $\sigma_{0.2}$ [MPa]	**Ultimate tensile strength σ_{UTS} [MPa]**	**Elongation ε_{max}[%]**
Base Material	299	392	17.3
FSW-Joint	237	329	6.8

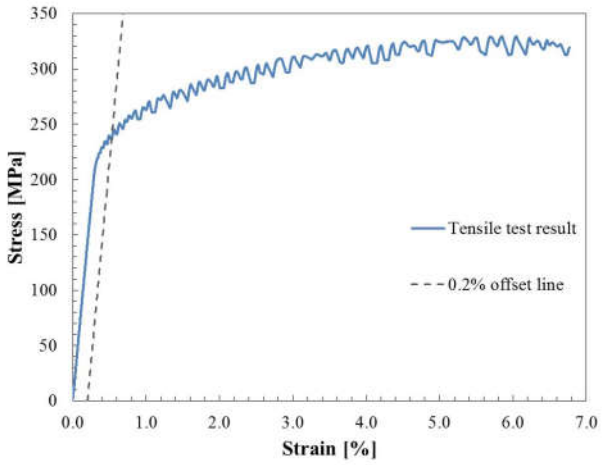

Fig. 1 Stress-strain curve of FSW joint obtained with a laser extensometer (gage length l_0 = 30 mm).

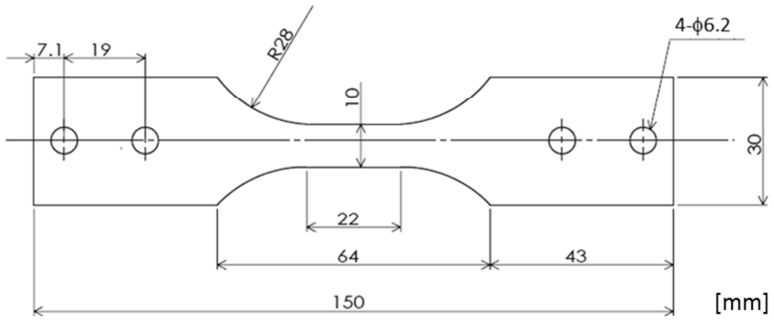

Fig. 2 Fatigue specimen geometry.

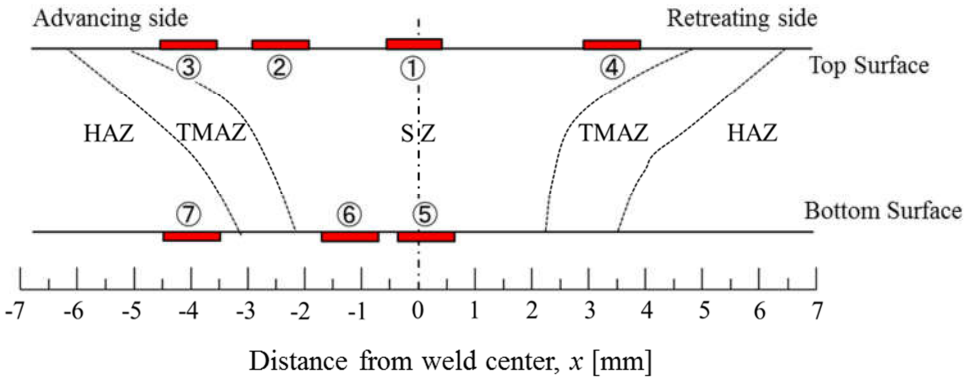

Fig. 3 Schematic illustration of strain gage locations.

Table 3 Strain gage locations

	Distance from weld center, x [mm]				
Weld feature	HAZ	SZ			
Top surface		③ -4.1	② -2.4	① -0.1	④ +3.4
Bottom surface	⑦ -4.0		⑥ -1.2	⑤ +0.1	

3. Results and discussion

3.1 Local straining behavior under monotonic loading

Fig. 4(a) and (b) show a macrosection of the weld structure and the two-dimensional hardness map of the FSW-joint, respectively. As seen in Fig. 4(a), the FSW joint shows a characteristically asymmetric weld structure mainly consisting of stir zone (SZ) and thermo-mechanically affected zone (TMAZ). Vickers hardness HV0.3 was measured on the cross section of the weld using a grid with distances of 250 µm both in width and thickness direction. The obtained two-dimensional hardness map is shown in Fig. 4(b). While the nominal hardness of the base material is about 111 HV0.3, pronounced softening can be observed in the weld part. According to the observation by Lapasset et al. [32], the existence of a heat affected zone (HAZ) in FSWed Al-Mg-Sc alloys is debatable. Nevertheless, as seen in the hardness map, a softened area was distributed even further on the outer side of TMAZ. Therefore, in this study this area is referred to as HAZ. Further details of the microstructure and hardness distribution can be found in our previous work [20] where the so called H-sample represents the welding conditions used in our current study.

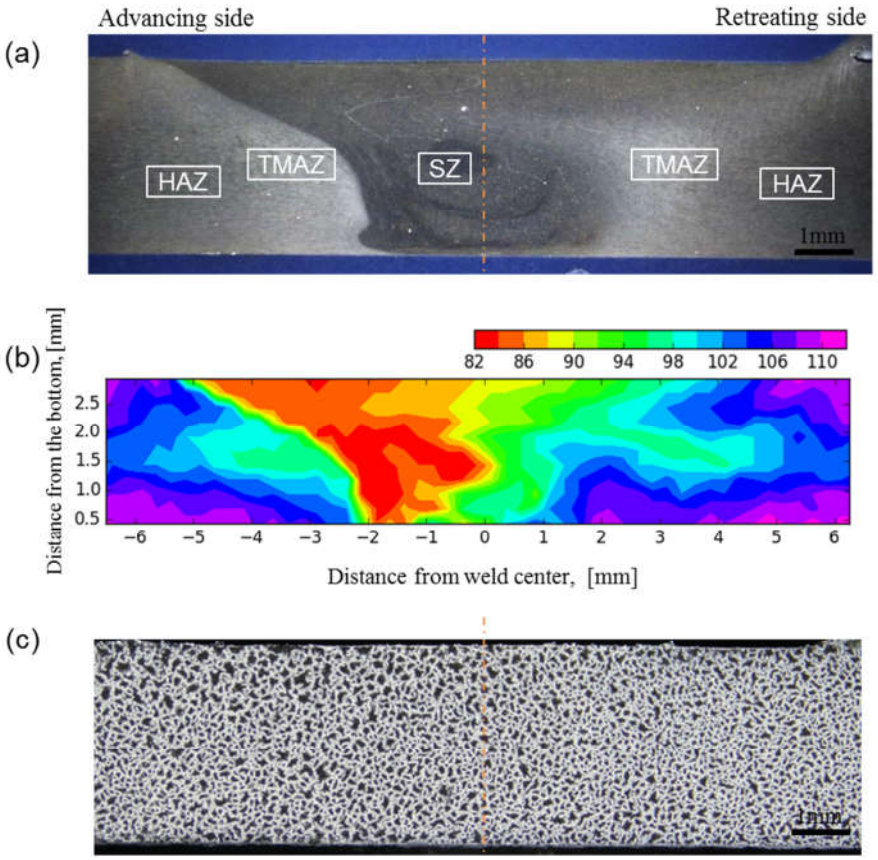

Fig. 4 Al-Mg-Sc FSW joint. (a) Macroscopic view of cross section of FSW joint, (b) hardness map and (c) random pattern painted on the side surface of the weld joint for DIC-based strain analysis.

For DIC-based local strain evaluation, the initial random pattern was painted on the side surface of the weld joint as seen in Fig. 4(c). Images of the side surface of the specimen were captured at a constant time interval of 6s, while the loading level was changing under a constant crosshead speed of 0.5 mm/min. The resulting imaging timing against the nominal stress is shown in Fig. 5, where data points up to 100s were depicted. The stress-time curve is linear at low stress levels, but around 200 MPa it starts to deviate from the linear line. 0.2% yield stress of this weld joint is 237 MPa as obtained by the laser extensometer measurement.

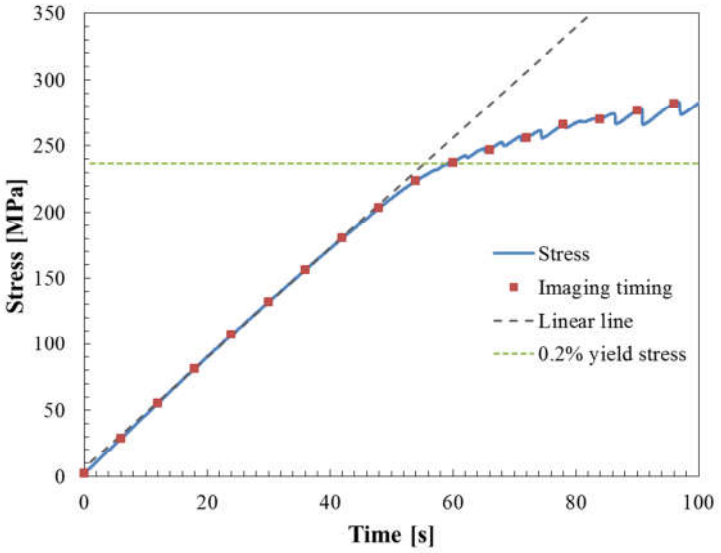

Fig. 5 Stress-time curve and imaging timing for DIC-based strain measurement.

Fig. 6 shows development of the local strain distribution from 36s to 66s; i.e. from the macroscopically elastic regime to the point beyond the 0.2% yield stress. The color bar of strain for these images is constant. The loading direction is in the negative X-direction in these images and the welding direction corresponds to the Z-direction, i.e. it is vertical to the page. The strain evaluated here is ε_x component

corresponding to the highest principal stress (at least during the elastic regime) in such a uniaxial tensile test. Boundary between SZ and TMAZ on the advancing side is schematically drawn in each strain map image (dashed line) as a reference.

In Fig. 6(b) at 36s the applied stress reaches 156 MPa, and the local strain distribution was almost uniform. Its average value was about 0.2%, which is comparably close to the value estimated with the macroscopic Young's modulus of this weld joint (72.2 GPa). At 48s with the applied stress level of 203 MPa, Fig.6(d), the first pronounced strain concentration is observed in an area in the lower SZ on the advancing side marked as A in Fig. 6(a). This first strain concentration took place around the softest part in the weld (see Fig. 4(b)). The strain in this area reached about 0.5 %. As seen in Fig.1 of the stress-strain curve obtained by the laser extensometer technique, the material was already fully yielding at a total strain value of 0.5%. Thus, it can be considered that this 0.5% strained region in Fig. 6(d) showed already local yielding for a nominal loading of 203 MPa.

In the next step at 54s with 223 MPa, the concentrated straining area clearly expanded towards top surface along the boundary between SZ and TMAZ on the advancing side. As seen in Fig. 5, the material started to deform nonlinearly at this applied stress level. It can be concluded that this local straining was the precursor of the global plastic deformation of the material. The strain around this area increased further during the following load steps. When the applied stress exceeded the macroscopic 0.2% yield stress at 66s, the strain in Area B increased more than that in Area A and the concentrated local strain in the region between Area A and B became highly pronounced.

The local straining behavior in the next steps after the macroscopic 0.2% yield stress is summarized in Fig. 7 (please consider individual scaling). The local strain in the region A-B along the boundary between SZ and TMAZ further increased as the applied load increased (see Fig. 7(a)), while this straining zone didn't expand into the adjacent TMAZ. At the same time, strong increase in strain was observed in the region from A towards the center of the weld joint on the top surface denoted as C in Fig. 7(a). The high straining zone became wider in SZ with increasing applied stress levels (Fig. 7(b) and (c)). The strain in Area A

near the bottom surface was still increasing at 240s and the strain around Area C on the top surface finally became higher than that at Area B (region of initially lowest hardness, see Fig. 4(b)). The strain at Area C as well as Area A continued to increase further and finally the specimen fractured along the region A-C.

The strain in TMAZ didn't become as high as in SZ, although the initial strain concentration occurred near the boundary of SZ and TMAZ. Thus, TMAZ seems to have higher deformation resistance i.e. higher yield stress than SZ, as also indicated by the initial hardness plot in Fig. 4(b). The initial concentrated strain was observed near the area with the lowest hardness (Fig. 4(b)). Area B where high strain was observed next to Area A also had low hardness, but the strain couldn't continue increasing due to the neighboring TMAZ with its constraining high deformation resistance. Initially, Area C which became a part of final fracture path was harder than Area B, but located in SZ apart from TMAZ boundary. Therefore, in this area continuation of deformation was possible with increasing load. Thus, most straining was concentrated in and restricted to SZ where remarkable softening was brought about by the FSW process.

However the straining and yielding didn't take place evenly in the whole SZ due to its heterogeneous microstructure and hardness distribution. These observations clearly indicate that the damage evolution during quasi-static failure cannot directly be "predicted" based on the initial local hardness distribution. Only the initial onset of plastic flow correlates well with the region of lowest hardness, whereas the following evolution of plastic straining is significantly affected by constraining effects of adjacent harder regions as well as local stress redistribution caused by the inhomogeneous plastic deformation.

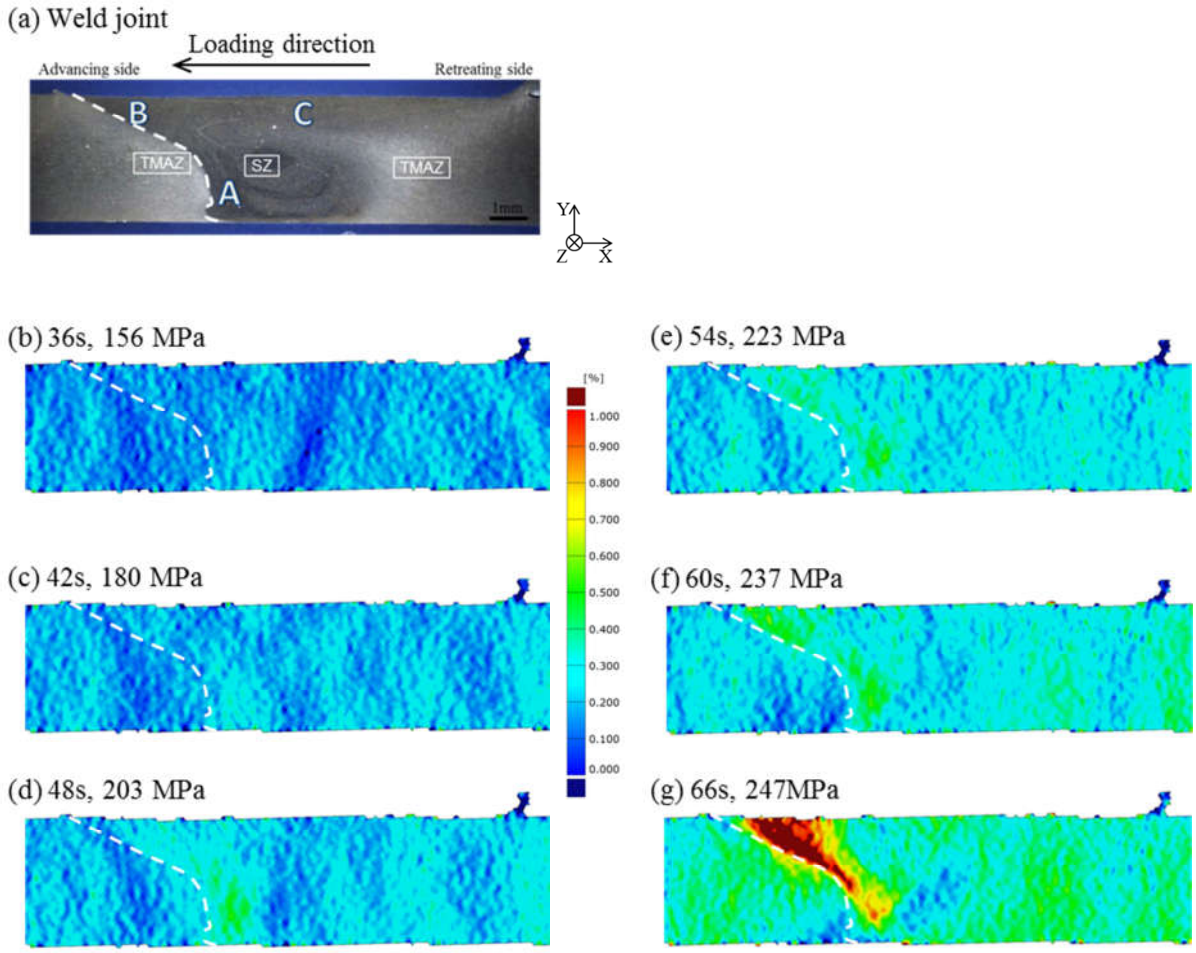

Fig. 6 Local strain development under tensile monotonic loading (up to the applied stress of 247 MPa); as seen in (a) the dashed line indicates the boundary between TMAZ and SZ.

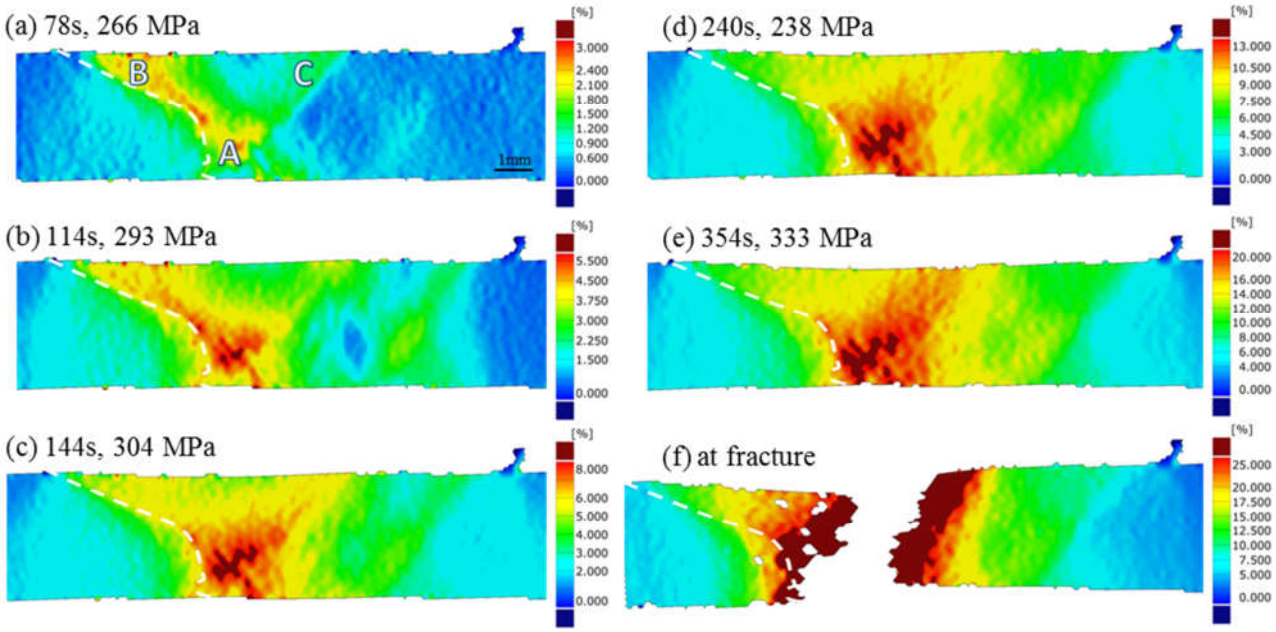

Fig. 7 Local strain development under tensile monotonic loading (after onset of yielding and up to fracture).3.2 Fatigue behavior

3.2.1 Fatigue strength of FSW joint

Fatigue lives of the FSW joint investigated in this study and that of the base material are listed in Table 4. Here, multiple specimens were tested at the same stress level (σ_a = 220 MPa) for the FSW joint, while one data point was obtained in the base material as reference. The fatigue lives of the FSW joints at the constant stress level of 220 MPa scattered significantly ranging from about 1.5×10^4 to 1.1×10^5 cycles and exhibited lower values than that of the base material. Please note that even the single fatigue data point of the base material may give a rough estimation of its fatigue strength as it is likely to represent a suitable estimate for the 50% probability of survival at the given stress level. Fractography showed that the shortest life was attributed to coalescence of two cracks. The other specimens fractured with single crack initiation and propagation as generally observed in HCF. As mentioned in the previous section, the hardness of the weld seam was lower than the base material (see Fig. 4(b)), and the tensile fracture

occurred basically in this region (see Fig. 7). Consistently, the fatigue strength of the FSW joint is also slightly lower than that of the base material.

Table 4 Fatigue lives of FSW joints and base material tested at σ_a=220MPa.

Material	Stress amplitude, σ_a [MPa]	No. of cycles to failure, N_f [-]
FSW joint	220	14,959
		35,650
		57,283
		61,693
		77,047
		114,376
Base material	220	159,350

3.2.2 Cyclic stress-strain behavior

Cyclic stress-strain behaviors were monitored during cyclic loading at the locations shown in Fig. 3 and Table 3, respectively. Please note that the strain measured here was an average value in the area ±0.5mm (in X-direction) around the measurement location because of the strain gages' 1 mm gage length. Fig. 8 shows overviews of the local cyclic stress-strain behavior at each location from the 2nd cycle where full cyclic loading was firstly applied. In these diagrams local strain was plotted with the macroscopically applied (i.e. nominal) stress. Fig. 8(a) shows the cyclic stress-strain curves at Location (1) around the center of the weld (i.e. in the SZ) on the top surface. Even in the very beginning of the cyclic loading phase (at 2nd cycle), a wide hysteresis loop was observed. This means that plastic deformation occurred locally at this measuring location covering a length of at least about 1 mm. The width of the hysteresis loops became smaller as the number of load cycles increased. Finally, at 5,000 cycles the cyclic stress-strain response became fully elastic. Similar behavior was observed at Location (2) and (3) on the top

surface of the advancing side as seen in Fig. 8(b) and (c) respectively, but with much lower plastic strains. At Location (4) (Fig. 8(d)) on the retreating side on the top surface the cyclic stress-strain behavior was almost elastic from the beginning of fatigue loading clearly reflecting the much higher hardness values in this region (see Fig. 4(b)). On the bottom surface, the cyclic local strain was measured at three locations: Location (5) at the weld center, Location (6) 1.2 mm apart from the weld center (still within SZ) on the advancing side and Location (7) in HAZ. In contrast to Location (1), only hardly pronounced plastic strain was detected at Location (5) at the weld center on the bottom surface (Fig. 8(e)). However wider hysteresis loops were observed at Location (6) as seen in Fig. 8(f) with plastic strain values comparably similar to that observed for Location (1). At Location (7) the cyclic strain behavior exhibited almost elastic straining similar to the findings at Location (4). After all, pronounced cyclic plastic straining was observed at 5 out of 7 locations. They were all found on the advancing side or at the weld center in SZ and three of them were located on the top surface.

The evolution of the cyclic plastic strain range $\Delta\varepsilon_p$ was examined in more detail. The cyclic plastic strain range can be evaluated by reading the strain range of those hysteresis loops at stress = 0 MPa for fully cyclic loading R = -1 (see Fig. 8(a) as an example of measuring $\Delta\varepsilon_p$). The obtained results are shown in Fig. 9. The highest maximum plastic strain range was observed at Location (1) and the second was found at Location (6) followed by Location (3). The plastic strain range at these locations reached its maximum in the early phase of the cyclic loading (at 2nd or 3rd cycle) and decreased gradually after the peak. At Location (2) and (5), their maximum values of plastic strain range were obtained later at 25 cycles and 80 cycles, respectively, with values much lower than that of the other locations. As seen in the DIC-based local strain measurement results under (quasi-) static tensile loading shown in Fig. 6, the first onset of yielding was observed slightly below the bottom surface denoted as Area A in Fig. 5. Location (6) was on the bottom surface but rather it is considered to correspond to Area A, because the fatigue specimens were prepared by removing both surface layers to avoid undesirable crack initiation from the surface asperities produced during the FSW process such as flashes and tool marks, as mentioned in section 2. Thus, it can be assumed that the locally low yielding stress at Location (6) brought about such high cyclic plastic

straining. Similarly, the high cyclic plastic strain observed at Location (3) can be attributed to the locally low yield stress around Area B as seen in Fig. 6. In contrast, Area C didn't show significant strain concentration for loadings below the macroscopic yield stresses in the tensile test. But from the result that the increasing straining at Area C in the following loading steps caused final fracture (see Fig. 7), it can be considered that this area could also be a preferable point of local cyclic straining, and consequently, a wide hysteresis loop was observed at Location (1). Summarized, local strain behavior in the tensile test shows some similarities with cyclic strain behavior in the fatigue test, but it doesn't apply to all behavior: e.g. although the most strain concentration was observed in Area A near the bottom surface in the tensile test, the highest cyclic plastic strain range was obtained at the weld center on the top surface near Area C.

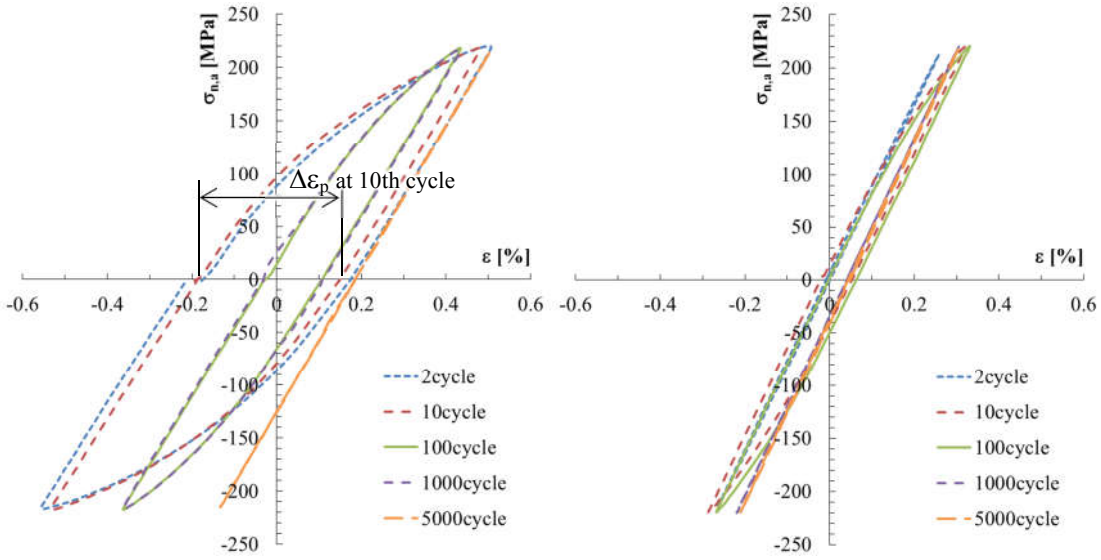

(a) Location (1)

(b) Location (2)

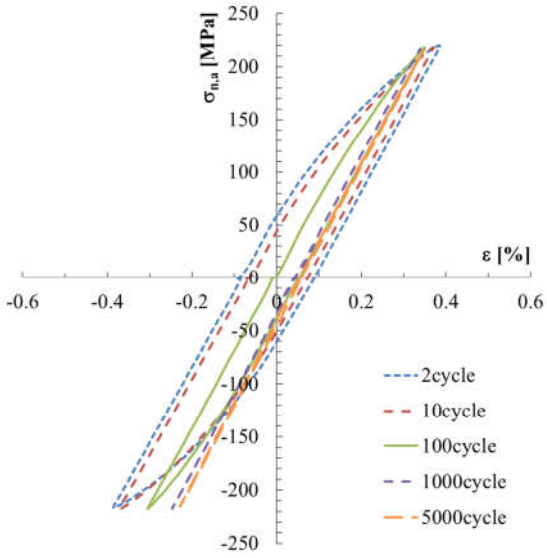

(c) Location (3)

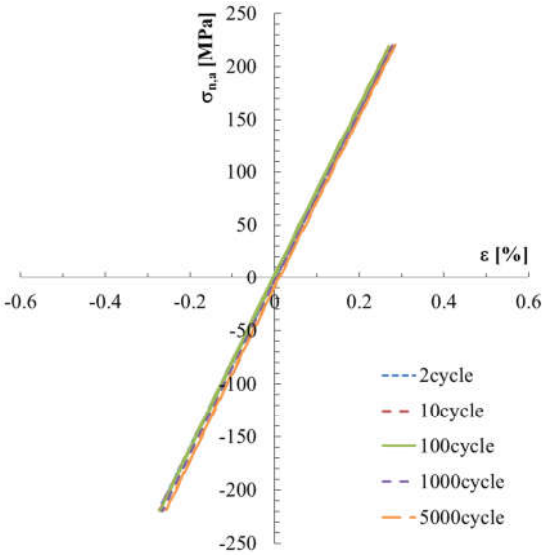

(d) Location (4)

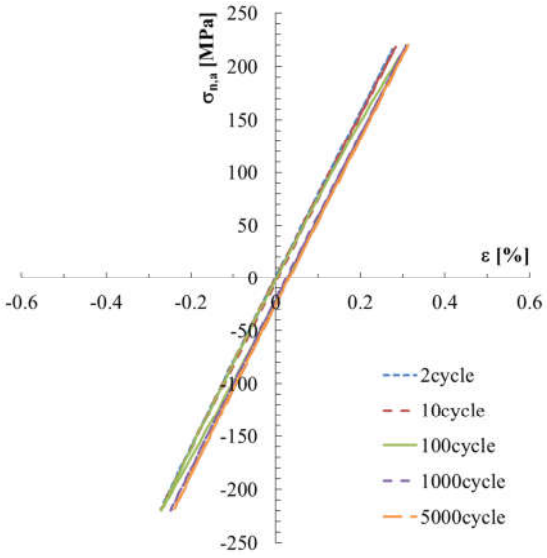

(e) Location (5)

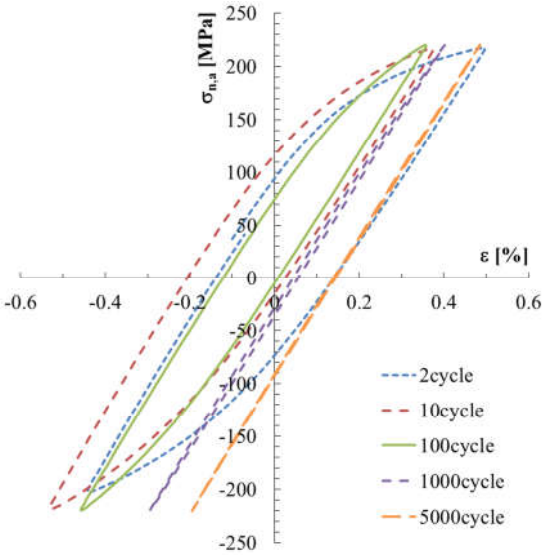

(f) Location (6)

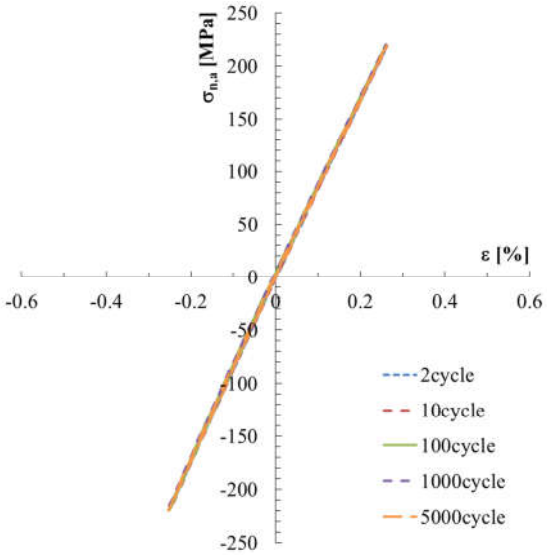

(g) Location (7)

Fig. 8 Local cyclic stress-strain behavior at Location (1) – (7) (1 – 5,000 cycles).

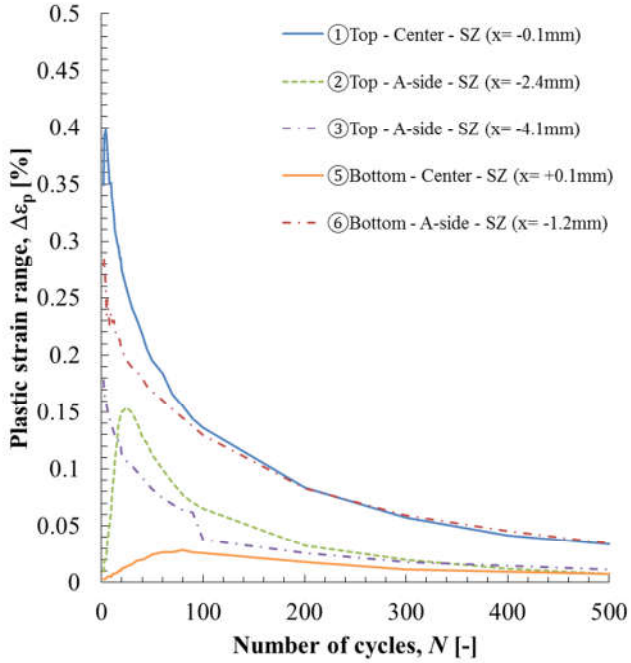

Fig. 9 Relationship between plastic strain range and number of cycles.

3.2.3 Crack initiation behavior

Fatigue crack initiation sites of the FSWed specimens tested at σ_a=220 MPa are schematically plotted in Fig. 10. One specimen fractured with coalescence of two cracks and the initiation site of the secondary crack is also plotted here. As seen in Table 4, the FSWed Al-Mg-Sc alloy showed widely scattered fatigue lives even when tested at the same stress amplitude. The color of symbols of the initiation sites indicates the range of fatigue lives according to the color bar on the right side of the image. The locations of the strain gages for the cyclic strain measurement are drawn in the image as well as their maximum plastic strain ranges. As seen in Fig. 10, crack initiation sites were distributed in SZ and in more detail the crack initiation sites of the main cracks as well as the secondary crack were found around the locations where relatively high cyclic plastic strain was observed. The cracks initiated at the location with the higher cyclic plastic strain generally showed the lower fatigue lives. As mentioned above, the cyclic plastic strain range reached its maximum in the early phase (~10 cycles) of fatigue as seen in Fig. 9 and then gradually decreased. After 5,000 cycles, local straining behavior at each observation location became almost elastic. Generally, in ductile materials, locally activated slip systems bring about fatigue crack initiation [33][34]. Since most fatigue crack initiations took place around the locations with the high cyclic plastic strain, it can be implied that formation of fatigue cracks was attributed to such high cyclic plastic strain in the early phase. However, except one specimen, the fatigue fracture was caused by initiation and propagation of only one main crack, although all the locations with the high cyclic plastic straining could have been potential crack initiation sites.

In this study, multiple crack initiations occurred around the weld center on the top surface in SZ near Location (1) and (2), where relatively high cyclic plastic strain was induced as there are no constraining “hard” regions such as TMAZ nearby. This sample with multiple crack initiation sites fractured due to coalescence of the two cracks resulting in the shortest fatigue life among 6 samples.

In another sample, one crack initiation was found around Location (3) on the top surface. This region was near the SZ/TMAZ boundary where concentrated strain in the tensile test was also observed for higher

loads as seen in Fig.6. The observed maximum cyclic plastic strain range in this region was the second lowest compared to the other crack initiation sites (higher than Location (2)). It showed the longest fatigue life among all. As observed in our past work on the fatigue behavior of FSWed Al-Mg-Sc alloys [20], the fatigue cracks propagated preferably in SZ, and TMAZ basically hindered their propagation. Due to the relatively low cyclic plastic strain and its location near the SZ/TMAZ boundary, it can be assumed that this crack required longer initiation and propagation lives than the others.

The bottom surface around Location (6), where first concentrated strain was observed in the tensile test, seems to be the most preferable crack initiation site. In fact, 4 out of 6 specimens had the crack initiation in the advancing side on the bottom surface close to Location (6). However, TMAZ was located close to those initiation sites and the maximum plastic strain generated during the cyclic loadings at Location (6) was lower than that of Location (1) (see Fig. 9). As a result, those samples had longer fatigue lives than that with the crack initiation around Location (1).

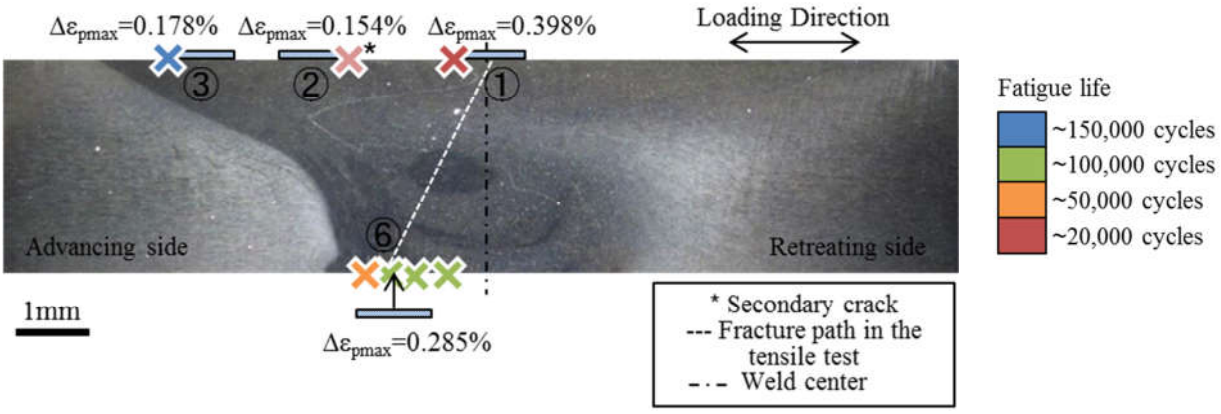

Fig. 10 Fatigue crack initiation sites and maximum cyclic plastic strain range tested at σ_a=220MPa.

As discussed above, local straining behavior under monotonically increasing loading was inhomogeneous within the weld and the deformation was not evenly developed during loading. The load-dependent local

strain evolution in the tensile test gave qualitative interpretation to some degree on local cyclic straining behavior under fatigue loading. However the actual cyclic straining behavior did not always coincide quantitatively to what could be expected from the local straining behavior under monotonic loading. In the present study, the applied stress amplitude was chosen as σ_a=220 MPa for all fatigue tests. To gain more insight into different crack initiation mechanisms, Fig. 11 shows additional crack initiation sites of the same materials tested at different stress amplitudes (results from our past work [20], in which the material was designated as H-specimen). As seen in Fig.12, also for different load levels fatigue crack initiation on the bottom surface was more likely than on the top surface. As shown in the SEM fractography of the same material tested at stress amplitudes of σ_a=200MPa and 240MPa (Fig. 12, taken from [20]), defect-like features were observed around the crack initiation sites on the bottom surface. Similar features were also observed in an FSWed Al-Mg-Sc alloy with different welding conditions, and it was considered as involution of the native oxide layer during the friction stir welding process [21]. Thus, it can be concluded that such frequent crack initiations on the bottom surface were attributed to the local high cyclic plastic straining in connection with the inhomogeneous microstructure due to the involution of the bottom oxide layer. It is also interesting to note here that in [20] crack initiation was also found on the retreating side in a specimen tested at σ_a=180 MPa. In this region, the hardness was high as seen in Fig. 4 and no concentrated strain was found in the tensile test in Fig. 6 and 7, but the microstructure was very complex as shown in Fig. 13 (taken from [20]). Cyclic straining behavior was not measured around this region unfortunately, but nevertheless according to the correlation between the monotonic and cyclic local straining behaviors discussed above, it can be assumed that significant plastic straining should be less likely to occur during cyclic loading especially at lower stress levels. Again, note that the local cyclic strain was measured with strain gages with a gage length of 1 mm in this study. This means that the local strain measured here was the averaged value in the gage area. Thus, regions with low cyclic straining values based on strain gage measurements could still include much higher but more localized straining within the gage area, and this could cause the crack initiation in the regions with a complex microstructure promoting locally inhomogeneous straining, as shown in Fig. 13.

Altogether, the local cyclic straining behavior taking the microstructures into account provides good correlation with the fatigue crack initiation behavior and the observed fatigue strengths. Thus, evaluation considering not only local cyclic straining response but also the microstructural influences and constraints is necessary to understand the fatigue behavior of material with complex heterogeneous microstructures such as friction stir welded alloys, since both fatigue crack initiation and early propagation behavior is strongly affected by the microstructures.

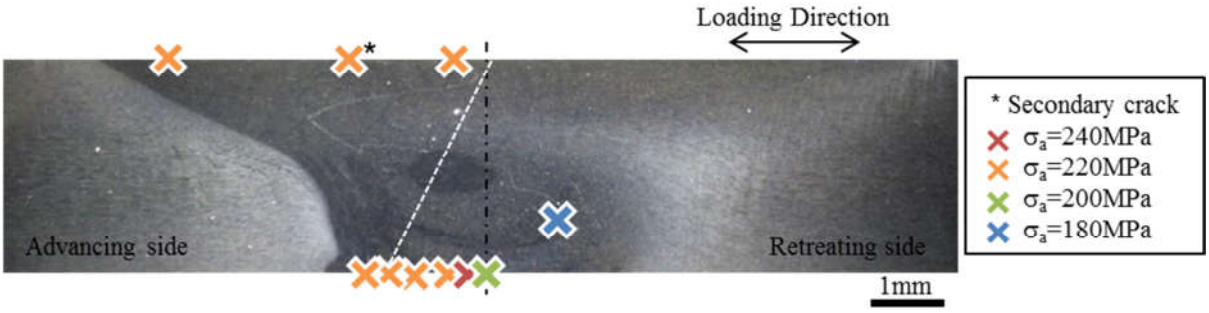

Fig. 11 Crack initiation sites tested at different stress amplitudes.

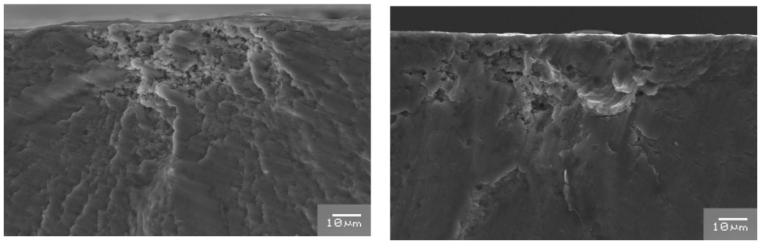

(a) σ_a=240 MPa **(b) σ_a=200 MPa**

Fig. 12 SEM observation at crack initiation sites on the bottom surface [20].

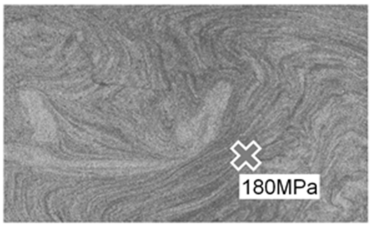

Fig. 13 Complex microstructure at fatigue crack initiation site tested at σ_a=180 MPa [20] .

4. Conclusions

Local straining behavior of a friction stir welded Al-Mg-Sc alloy was examined under monotonic and cyclic loadings. The FSWed Al-Mg-Sc alloy had heterogeneous microstructure in the weld consisting of a stir zone (SZ) and a thermo-mechanically affected zone (TMAZ). A digital image correlation (DIC) technique was employed for the local strain analysis under monotonic tensile loading. In-plane strain development on the side surface of the weld was observed in accordance with the applied stresses. Fully reversed (R = -1) fatigue tests were conducted at a constant stress amplitude of 220 MPa which was slightly lower than the macroscopic 0.2% yield stress of the welded material. Local cyclic stress-strain behavior during fatigue loading was measured at 7 different locations in the weld by means of a strain gage technique with a gage length of 1 mm.

Due to the limited number of experiments no statistically significant results can be provided. Nevertheless, as our observations provide a very consistent image of the damage evolution in FSW joints under tensile and fatigue loadings, the following conclusions can be drawn:

- Tensile testing: Due to the complex microstructure and hardness distribution in the FS weld neither the regions of minimum hardness nor the onset of initial plastic straining accurately predict the damage evolution until fracture.
- Fatigue testing: Cyclic plastic strain was found mainly on the advancing side of SZ. But it was observed only in the very early phase of fatigue loading. After about 5,000 load cycles at the latest no more plastic straining could be observed.
- Fatigue testing: Crack initiation took place generally around the areas where high cyclic plastic strain was observed. Thus, it can be concluded that the cyclic plastic strain in the early phase significantly contributed to the crack initiation behavior.

- Fatigue testing: Fatigue crack initiation on the bottom surface was often observed likely due to the high cyclic plastic strain in addition to the complex microstructure with the involution of the oxide layer found in our previous work [21].
- Neither the local hardness distribution nor the straining behavior under quasi-static tensile testing alone can predict the damage evolution or crack initiation sites under fatigue loading. But the local strain evolution under the monotonic loading provides qualitatively good correlation to the behavior of the cyclic strain development under fatigue loading.
- Overall, in this study the fatigue crack initiation behavior and fatigue lives could consistently be attributed to the local cyclic straining behavior and the heterogeneous microstructure.
- But to fully understand damage evolution under monotonic as well as cyclic loading it is mandatory to consider both local material properties and constraining effects of adjacent regions with varying properties. Furthermore, if additional stress concentrators such as hard phases or phases with weak boundaries exists (here resulting from oxide layer mentioned above) they must also be taken into account.

Acknowledgement

The authors would like to thank Mr. Sauer from the Institute for Materials Research of the German Aerospace Center in Germany for providing the FSW joints, and Mr. Ono, Mr. Matsuo and Mr. Ochiai from the department of mechanical engineering of Gifu University in Japan for the cyclic strain measurements.

References

[1] W.M. Thomas, E. D. Nicholas, J. C. Needham, M. G. Murch, P. Temple-Smith, C. J. Dawes: Improvements relating to friction welding. European Patent Specification EP 0 615 480 B1, 1992

[2] R.S. Mishra, Z.Y. Ma: Friction stir welding and processing, Reports: A Review Journal, Materials Science and Engineering R 50, 2005, pp. 1-78

[3] W.M. Thomas, E.D. Nicholas: Friction stir welding for the transportation industries, Materials & Design, 18, 1997, pp. 269-273

[4] T. Kawasaki, T. Makino, K. Masai, H.Ohba, Y. Ina, M. Ezumi: Application of Friction Stir Welding to Construction of Railway Vehicles, JSME International Journal, A47, 2004, pp. 502-511

[5] F. Delany, S.W. Kallee, M.J. Russell: Friction stir welding of aluminium ships, International Forum on Welding Technologies in the Shipping Industry (IFWT), 2007

[6] S.W. Kallee, E.D. Nicholas, W.M. Thomas: Industrialisation of friction stir welding for aerospace structures, Structures and Technologies – challenges for future launchers, third European Conference, 2001

[7] A. Grimm, S. Schulze, A. Silva, G. Göbel, J. Standfuss, B. Brenner, E. Beyer, U. Füssel: Friction stir welding of light metal for inductrial applications, Materials Today: Proceedings 2S, 2015, pp. S169-S178

[8] P.L. Threadgill: Terminology in friction stir welding, Science and Technology of Welding and Joining, 12, 2007, pp. 357-360

[9] G. Çam, S. Mistikoglu: Recent Development in Friction Stir Welding of Al-alloys, J. Materials Engineering and Performance, 23, 2014, pp. 1936-1953

[10] Y.S. Sato M. Urata, H. Kokawa: Parameters controlling microstructure and hardness during friction-stir welding of precipitation-hardenable aluminum alloy 6063, Metallurgical and Materials Transactions A, 33A, 2002, pp. 625-635

[11] J. Yan, M.A. Sutton, A.P. Reynolds: Process-structure-property relationships for nugget and heat affected zone regions of AA2524-T351 friction stir welds, Science and Technilogy of Welding and Joining, 10, 2005, pp. 725-736

[12] S.R. Ren, Z.Y. Ma, L.Q. Chen: Effect of welding parameters on tensile properties and fracture behavior of friction stir welded Al-Mg-Si alloy, Scripta Materialia, 56, 2007, pp. 69-72

[13] M. Jayaraman, R. Sivasubramanian, V. Balasubramanian: Establishing relationship between the base metal properties and friction stir welding process parameters of cast aluminium alloys, Materials and Design, 31, 2010, pp. 4567-4576

[14] W.D. Lockwood, B. Tomaz, A.P. Reynolds: Mechanical response of friction stir welded AA2024: experiment and modelling, Materials Science and Engineering A, A323, 2002, pp. 348-353

[15] C. Genevois, A. Deschamps, P. Vacher: Comparative study on local and global mechanical properties of 2024 T351, 2024 T6 and 5251 O friction stir welds, Materials Science and Engineering A, A415, 2006, pp. 162-170

[16] C. Leitão, I. Galvão, R.M. Leal, D.M. Rodrigues : Determination of local constitutive properties of aluminium friction stir welds using digital image correlation, Materials and Design, 33, 2012, pp. 69-74

[17] Z.H. Zhamg, W.Y. Li, Y. Feng, J.L. Li, Y.J. Chao: Global anisotropic response of friction stir welded 2024 aluminum sheets, Acta Meterialia, 92, 2015, pp. 117-125

[18] H. Li, Q.-L. Dai, Q.-Y. Shi: Experimental study on the heterogeneity of mechanical properties of friction stir welded joints with the digital image correlation method, Strength of Materials, 47, 2015, pp. 80-86

[19] C. Deng, R. Gao, B. Gong, T. Yin, Y. Liu: Correlation between micro-mechanical property and very high cycle fatigue (VHCF) crack initiation in friction stir welds of 7050 aluminum alloy, International Journal of Fatigue, 104, 2017, pp. 283-292

[20] M. Besel, Y. Besel, U. Alfaro Mercado, T. Kakiuchi, Y. Uematsu: Fatigue behavior of friction stir welded Al-Mg-Sc alloy, International Journal of Fatigue, 77, 2015, pp. 1-11

[21] Y. Besel, M. Besel, U. Alfaro Mercado, T. Kakiuchi, T. Hirata, Y. Uematsu: Influence of local fatigue damage evolution on crack initiation behavior in a friction stir welded Al-Mg-Sc alloy, International Journal of Fatigue, 99, 2017, pp. 151-162

[22] G. Tempus: New aluminium alloys and fuselage structures in aircraft design, Materials Day "Werkstoffe für Transport und Verkehr", ETH Zürich Switzerland, 2001

[23] Y.A. Filatov, V.I. Yelagin, V.V. Zakharov: New Al-Mg-Sc alloys, Materials Science & Engineering A, A280, 2000, pp. 97-101

[24] K.V. Jata, S.L. Semiatin: Continuous dynamic recrystallization during friction stir welding of high strength aluminum alloys, Scripta Materialia, 43, 2000, pp. 743-749

[25] B. Heinz, B. Skrotzki: Characterization of a Friction-Stir-Welded Aluminum Alloy 6013, Metallurgical and Materials Transactions B, 33B, 2002, pp.489-498

[26] J.-Q. Su, T.W. Nelson, R. Mishra, M. Mahoney: Microstructural investigation of friction stir welded 7050-T651 aluminium, Acta Materialia, 51, 2003, pp. 713-729

[27] G. Biallas, C.D. Donne, C. Juriçic: Monotonic and cyclic strength of friction stir welded aluminium joints, Advances in Mechanical Behaviour Plasticity and Damage, Proc. of EUROMAT, 1, 2000, pp. 115-120

[28] H.J. Liu, H. Fujii, M. Maeda, K. Nogi: Tensile properties and fracture locations of friction-stir-welded joints of 2017-T351 aluminum alloy, Journal of Materials Processing Technology, 142, 2003, pp.692-696

[29] Y.S. Sato, H. Takauchi, S.H.C. Park, H. Kokawa: Characteristics of the kissing-bond in friction stir welded Al alloy 1015, Materials Science and Engineering A, A405, 2005, pp.333-338

[30] A.H. Cottrell: LXXXVI. A note on the Protevin-Le Chatelier effect, Philosophical Magazine and Journal of Science, 44, 1953, pp. 829-832

[31] GOM GmbH; https://www.gom.com/ [accessed November 2018]

[32] G. Lapasset, Y. Girard, M.H. Campagnac, D. Boivin: Investigation of the microstructure and properties of a friction stir welded Al-Mg-Sc alloy, Materials Science Forum, 426-432, 2003, pp. 2987-2992

[33] M. Klesnil, P. Lukáš : Fatigue of metallic materials, Materials science monographs 7, Amsterdam, Elsevier Scientific Publishing Company, 1980

[34] S. Suresh: Fatigue of Materials second edition, New York, Cambridge university press, 1998